Trends in Mechanical Engineering & Technology

Volume - 16, Issue - 2, Year – 2026

ISSN No. : 2231-1793

Research Article

Received Date: 26th May, 2026

Accepted Date: 6th June, 2026

Published Date: 20 June, 2026

Analysis of Thermoelectric Generator for Automotive Exhaust Energy Recovery

Rone[1]*, Manjeet Singh[2]

[1,2]Department of Mechanical engineering, EIT FARIDABAD

***Corresponding author: ronie.somadder@gmail.com**

ABSTRACT: Utilizing waste heat from thermodynamic systems has shown to be a successful tactic for reducing environmental emissions and improving overall energy efficiency. About 40% of the chemical energy generated during fuel combustion is rejected by exhaust gases in internal combustion engines. It is possible to increase vehicle fuel efficiency and lower greenhouse gas emissions by harvesting this otherwise lost heat energy and turning it into useable electrical power. A viable answer for this kind of energy recovery is thermoelectric (TE) technology, which allows heat to be directly converted into electricity without the need for moving parts. Advantages of this technology include reduced maintenance needs, silent operation, and operational reliability. Despite these benefits, the large-scale application of automotive exhaust thermoelectric generators (AETEGs) remains constrained due to issues including temperature non-uniformity across modules, reduced conversion efficiency, and performance deterioration under variable engine operating conditions.

In order to evaluate system performance under simulated exhaust circumstances typical of a light-duty vehicle, an automotive exhaust thermoelectric generator and a special experimental test facility were devised and constructed. A box-style heat exchanger, segmented cooling plates, and 44 bismuth telluride thermoelectric modules positioned on either side of the heat exchanger comprise the developed AETEG. Voltage-current (V-I) and power-current (P-I) characteristics at various thermal input levels were used to experimentally assess system performance. The peak power production of each module and the pressure drops across the heat exchanger were also measured. Degradation at the cold-side thermoelectric leg–solder contact increased internal resistance and decreased power production, according to thermal cycling studies.

KEYWORDS: - Waste heat recovery, thermoelectric generator, automotive exhaust energy, heat exchanger design, thermoelectric power generation

1. INTRODUCTION

For automobile exhaust heat recovery, thermoelectric generator (TEG) systems usually comprise arrays of thermoelectric modules placed between cooling plates and a heat exchanger. Automotive exhaust thermoelectric generators (AETEGs) are a promising concept, but there are a number of technical obstacles in their development. These include relatively low thermoelectric conversion efficiency, varying exhaust gas conditions, non-uniform temperature distribution across the heat exchanger surface, limited heat exchanger performance because of structural limitations, and issues with long-term operational reliability.

The efficacy of the heat exchanger and the thermoelectric modules' conversion efficiency are the main factors that determine an AETEG's overall efficiency. Depending on where each module is located in the array, uneven exhaust gas flow inside the heat exchanger frequently results in non-uniform temperature distribution. Temperature mismatch conditions thus arise, which affect the modules' electrical functioning point when coupled, resulting in decreased power output. Although a variety of flow-control structures, including baffles, diffusers, and flow straighteners, are frequently employed to enhance flow distribution, careful geometric optimization of these elements is required to improve temperature uniformity. The temperature reduction of exhaust gases along the flow direction as a result of heat extraction by the modules is another significant aspect influencing system performance. As a result, the thermoelectric materials only get a small portion of the available heat, which leads to a lower practical efficiency than theoretical material efficiency.

2. LITERATURE REVIEW

2.1. Energy recovery techniques: -

In order to recover energy from cars that would otherwise be lost during operation, a number of solutions have been proposed. When needed, the recovered energy can be stored and then delivered to various vehicle subsystems. Such energy recovery systems should ideally run continuously while guaranteeing that the energy is efficiently delivered when needed and stored with few losses. These systems must meet practical design requirements in addition to having great energy conversion and storage efficiency. To prevent adding to the vehicle's total bulk or packing restrictions, they should be lightweight and take up as little space as possible. Reducing parasitic losses and ensuring that the energy recovery mechanism does not adversely impact the vehicle's overall performance and fuel efficiency are two benefits of maintaining a lightweight and compact design.

2.2. Classification of energy recovery techniques

The type of energy being recovered, the source of wasted energy, and the particular conversion technology used can all be used to categories energy recovery solutions in cars [1]. These categories aid in determining appropriate strategies for enhancing vehicle energy efficiency.

Generally speaking, exhaust heat, braking systems, vibrations, and aerodynamic losses are the main causes of the wasted energy found in automobiles. This lost energy may be transformed into mechanical, thermal, or electrical energy that can be utilized by various vehicle subsystems, depending on the recovery process.

This wasted energy is captured and transformed using a variety of conversion technologies, such as organic Rankine cycle systems, thermoelectric generators, regenerative braking systems, and turbo-compounding devices. Regarding efficiency, complexity, cost, and viability of integration within current vehicle architectures, each method has pros and cons of its own. Researchers can more accurately assess these technologies' potential to increase overall vehicle efficiency and lower fuel consumption by classifying them according to energy source and conversion method.

Figure 2.1 illustrates the classification of major energy recovery techniques currently being explored in modern automotive systems.

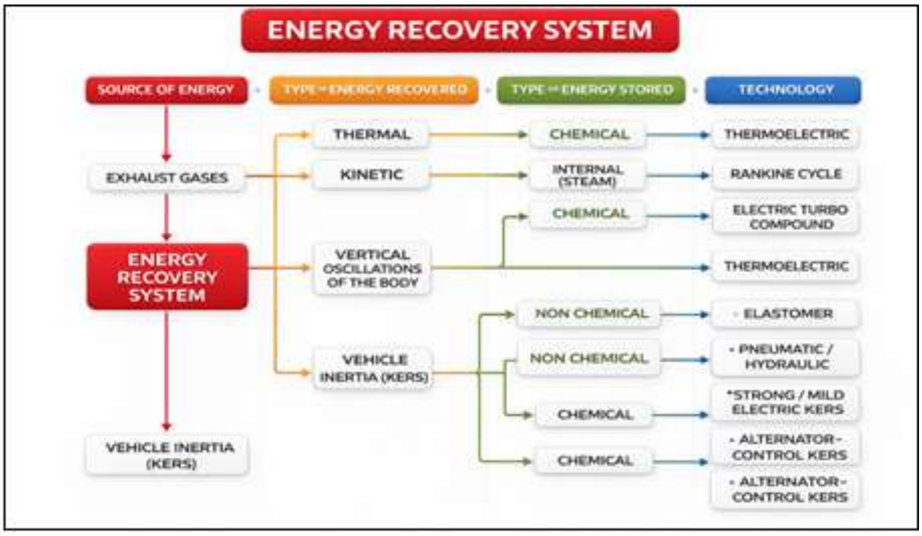

Fig. 2.1 Classification of energy recovery techniques envisaged in automobiles

Exhaust gases, vehicle inertia, and vertical oscillations are the sources from which energy can be recovered in an automobile system. Both thermal and kinetic recovery are possible from the exhaust gases. In the former, TE technology is used to directly transform the heat present in the exhaust gas into electrical energy. In the latter, Rankine cycle or electric turbo-compounding (ETC) technologies are used to transform the exhaust gas's kinetic energy (KE) into mechanical and/or electrical energy. By using regenerative braking, the kinetic energy recovery system (KERS) transforms KE that would have been wasted as heat during braking into forms that may be used. KERS is further categorized according on the conversion method. Pneumatic and hydraulic KERS store KE as pressure energy, whereas elastomer or spring KERS store KE as elastic energy. In both situations, the stored energy is released as electrical or mechanical energy. KE is transformed into rotational energy in flywheel-based KERS and released as mechanical energy as needed. Additionally, there are alternator-control and electric KERS, which use a motor-generator system to convert KE to electrical energy.

3. EXPERIMENTAL METHODOLOGY

3.1. Design and fabrication of automotive exhaust thermoelectric generator (AETEG)

The AETEG experimental setup includes cooler plates to remove heat from the cold side of the TE modules, a heat exchanger to collect heat from the hot flowing gas and TE modules to transform the heat into electricity. Figure 3.1 depicts a schematic of the AETEG configuration utilized in this work. On both the top and bottom sides of the heat exchanger, the TE modules were positioned between the heat exchanger and the cooler plates.

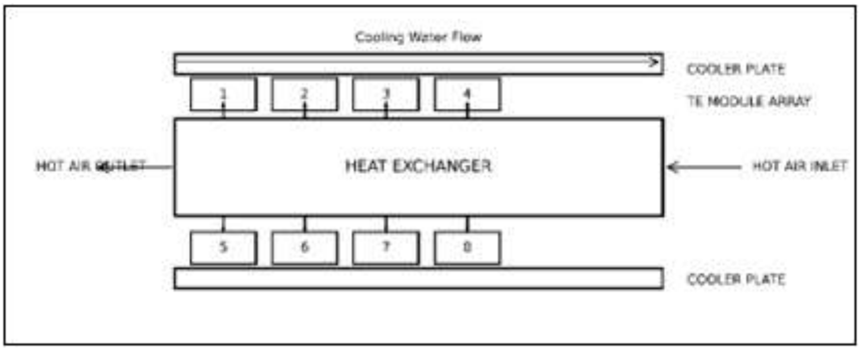

Fig. 3.1 Schematic of the arrangement of the AETEG.

3.2. Heat exchanger

The heat exchanger was constructed from stainless steel (SS 304) with a rectangular cross-section and a thickness of 2 mm. The channel's external measurements were 250 x 200 x 100 mm. The ends were joined to the hot air pipe by flanged couplings using truncated rectangular pyramids, each measuring 100 mm in length. The heat exchanger's comprehensive drawing with all of its dimensions is shown in Figure 3.2.

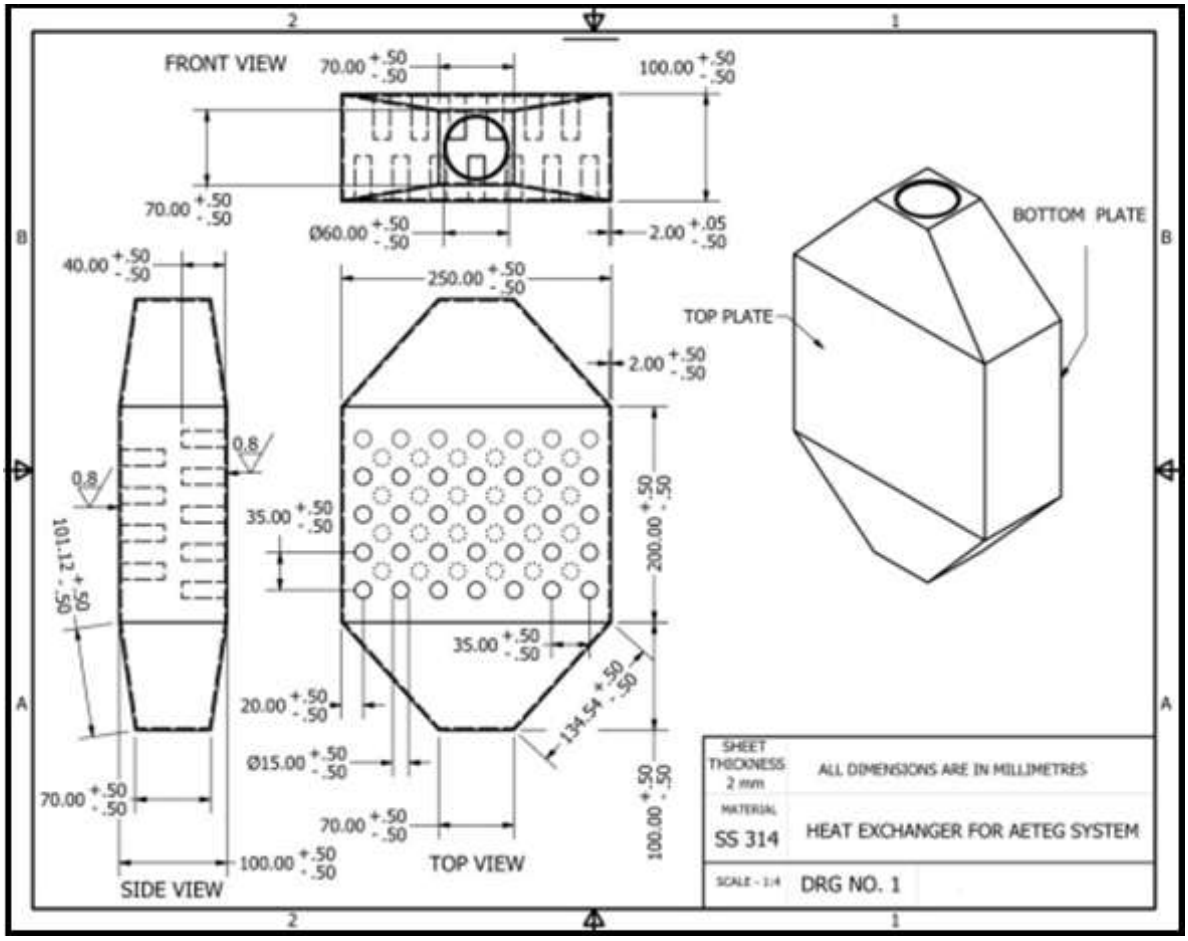

Fig. 3.2 Dimensions of the heat exchanger channel and the pin fin arrangement in it

To improve the heat extraction from hot air, pin fin arrays were welded in-line to the inner surface of the rectangular channel using TIG welding. Within a particular heat exchanger volume, pin fins are among the most efficient heat transfer structures [1]. When compared to a smooth channel, the addition of pin fins increases the heat transfer coefficient by 50–100% when the Reynolds number is ≤ 20,000 [2]. Several pin cross-sections have been used to study the augmentation using these internal structures, with circular pin cross-sections being the most popular. Drop-shaped [1], elliptical [2], square [3], and other cross-sections were also examined. At higher Reynolds numbers (Re ≥ 10000), the fin shapes have less of an effect on the heat transfer properties [4]. There are two common arrangements for the pin fins: staggered and in-line. Because of their greater heat transfer capacity, metal pin fin arrays utilized in the integrated thermoelectric system performed better with staggered arrays than with in-line arrays [5]. On the other hand, the pressure drop in the staggered design is relatively bigger [6] [7]. Circular cross-section pin fins were chosen for the current heat exchanger design because they are easier to produce and offer a better trade-off between heat transfer and pressure loss than alternative cross-sections. The pin fin configuration of the heat exchanger intended for this investigation is depicted in Figure 3.3. The pin fins were positioned in a straight line. In relation to the top plate array, the fin array on the heat exchanger's bottom plate was positioned offset. The height to diameter (H/D) ratio of the pin fin was maintained at 2.7 and the stream-wise pitch to diameter ratio (ST/D) and the span-wise pitch to diameter (SP/D) ratio of the pin fin array was 3.3. L and W represent the length and width of the rectangular channel, respectively.

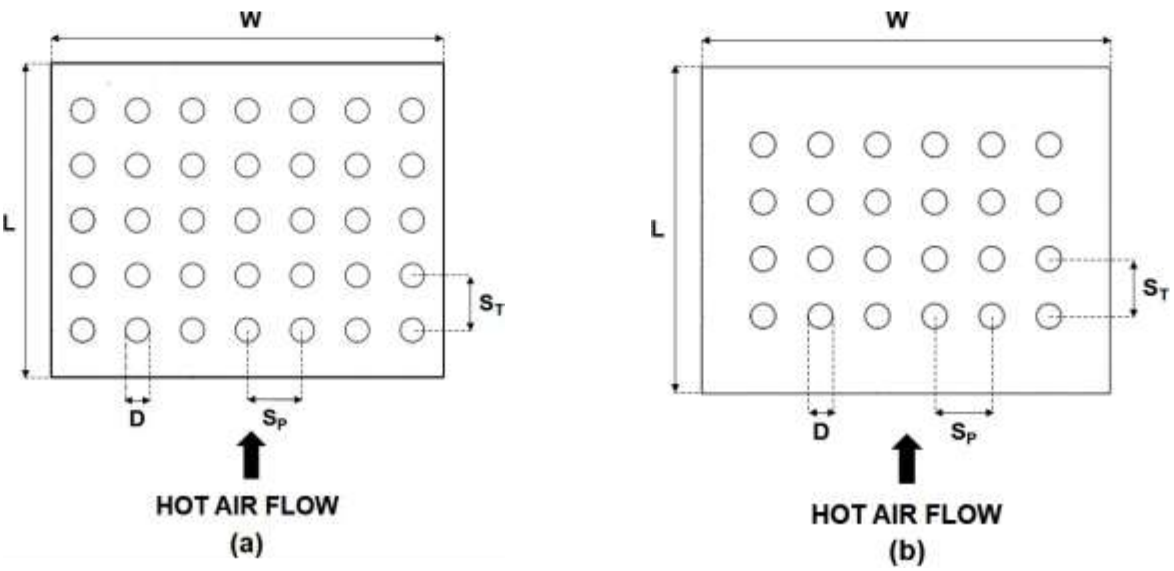

Fig. 3.3 Pin fin arrangement on the (a) top plate and (b) bottom plate of the heat exchanger

The actual photos of the heat exchanger and its inside are displayed in Figure 3.4. The fin arrangement in the rectangular channel is depicted in Figure 3.4 (a). Tungsten inert gas (TIG) welding was used to attach the pins to the rectangular channel's inner surface [8]. A 50 mm length SS (SS 316) pipe with an inner diameter of 50.8 mm was used to secure the ends of the truncated rectangular pyramids on both sides. To connect the hot air pipe coming from the heat source, an SS 316 flange (ANSI, slip on the raised face (SORF) of class 150) was welded at one end. The other end was also welded with a similar flange to connect to the outlet pipe (figure 3.4 (b)). A 2 mm thick SS plate with 30% area perforated was kept on the inlet region of the rectangular channel to straighten the hot air flow (figure 3.4 (c)).

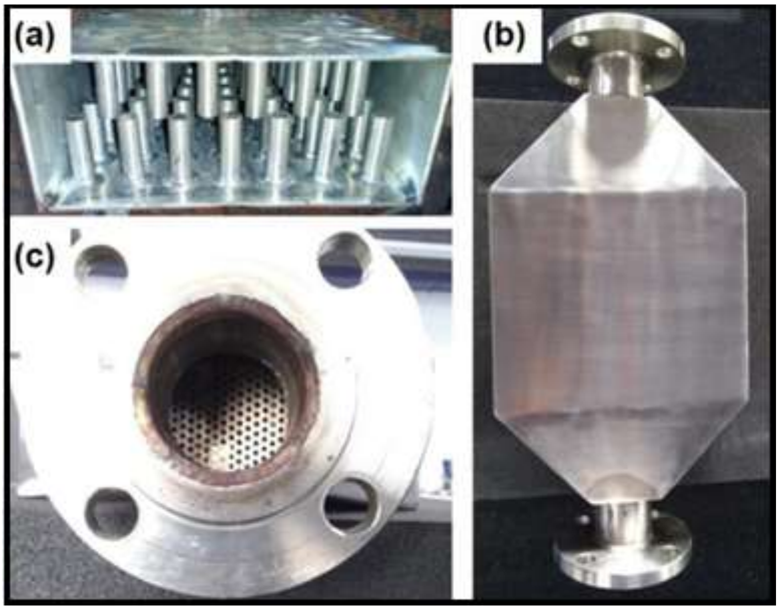

Fig. 3.4 Actual images of the (a) pin fin arrays (b) heat exchanger (c) perforated plate at the inlet of the rectangular channel

3.3. Cooler plate

Cooler plates were used to extract heat from the TE modules' cold side. The cooler plate was made of a 2 mm thick SS 316 sheet and had external dimensions of 250 mm × 200 mm × 40 mm. Four equal parts made up the internal volume (figure 3.5). Three baffles, each measuring 40 mm in height and 75 mm in length, were installed in each segment to allow the coolant to flow in a serpentine pattern. The steel base plate was welded to the 2 mm thick baffles, which were sealed with a rubber gasket on top. Additionally, each portion had a 20 mm-diameter coolant input and outlet. The true image of the SS cooler plate is displayed in Figure 3.6. After the TE modules were positioned, two similar cooler plates were positioned, one on the heat exchanger's top and another on its bottom flat surface. The test setup had two water heads, one for each of the two cooler plates' inlets and exits.

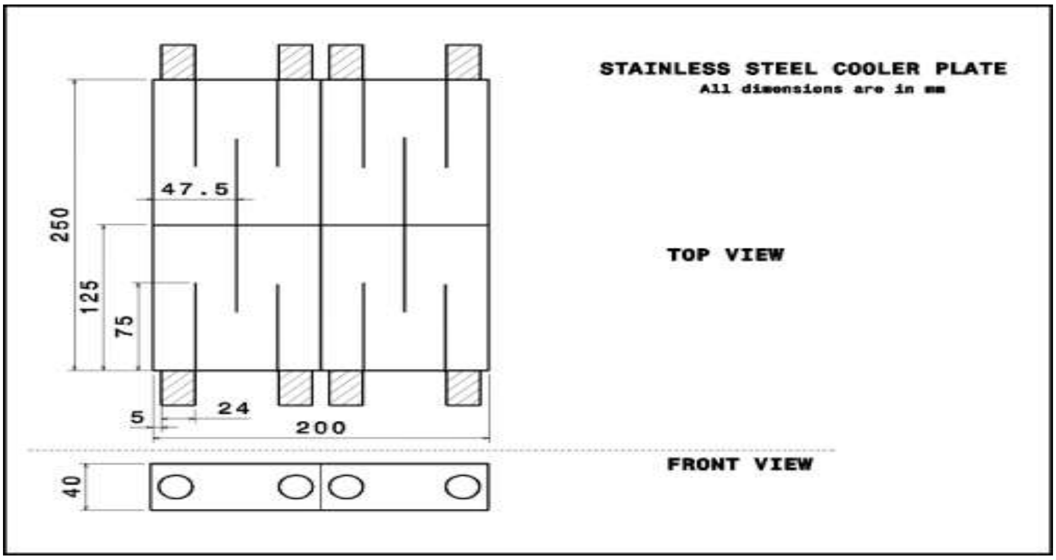

Fig. 3.5 Drawing of the stainless-steel cooler plate

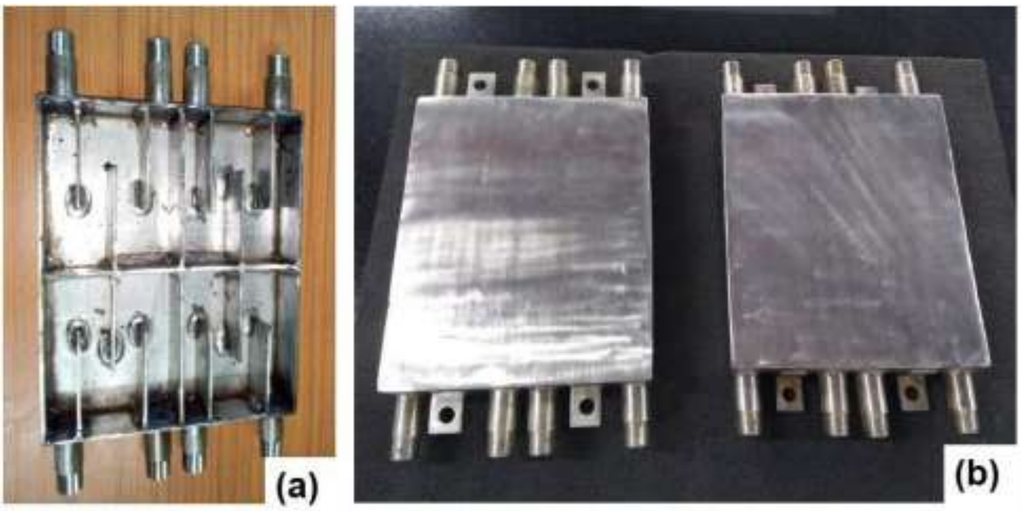

Fig. 3.6 Actual image of the (a) baffles in the cooler plate (b) fabricated cooler plate Pin fin arrangement on the (a) top plate and (b) bottom plate of the heat exchanger

4. EXPERIMENTAL SETUP

Eight TE modules in AETEG were used for the thermal cycling investigations. They were arranged symmetrically on the heat exchanger's upper surface (Figure 4.1(a)), which was covered by the aluminum cooler plate. Each of the TE modules was positioned in a distinct temperature gradient on the heat exchanger's surface. Figure 4.1(b) depicts the actual configuration of the TE modules on the heat exchanger surface.

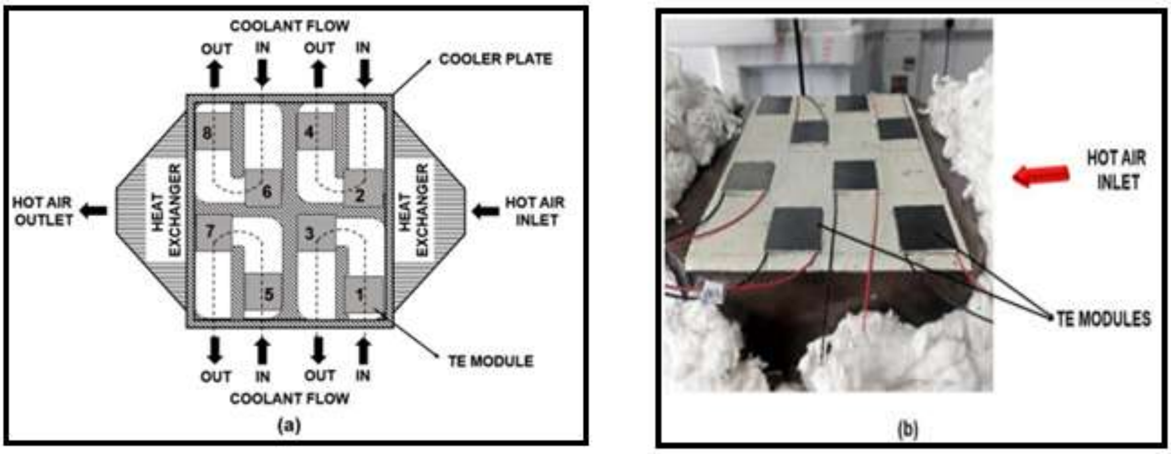

Fig. 4.1 (a) Schematic of arrangement of eight TE modules on the surface of the heat exchanger (b) Actual image of the arrangement.

4.1. Internal resistance and V-I characteristics of the TE modules before cycling

Prior to the thermal cycling experiments, the R_{int} at room temperature (RT resistance), V-I characteristics, and HT resistance of each individual TE module in AETEG were ascertained [9]. After the TEG system achieved the steady-state condition for a heater set temperature (THST) that matched the holding temperature of each thermal cycling profile (TCP), the VOC and V-I characteristics were ascertained.

4.2. Thermal cycling experiments

Three TCPs were used for the heat cycling studies. The TEG assembly in each instance used a set of eight new TE modules. Coolant temperature and flow rate, air temperature, and air flow rate were the variables that could be changed separately in the test rig [10]. The TCPs in this study were produced by changing the temperature of the heat source at various heating rates while maintaining a constant input air flow rate to the heater. The aluminum coolant plate's coolant temperature and flow rate were maintained at 25 l/min and 16ºC, respectively. Typical trend displays include:

- TC1 / TC2 → Temperature sensor readings
- STUD / STUM → Upper and middle surface temperatures
- GTU / GTM → Gas temperature measurements
- FLOW → Fluid flow rate
- PRESSURE → System pressure
- DPT → Differential pressure
- DC LOAD → Electrical load applied to thermoelectric modules

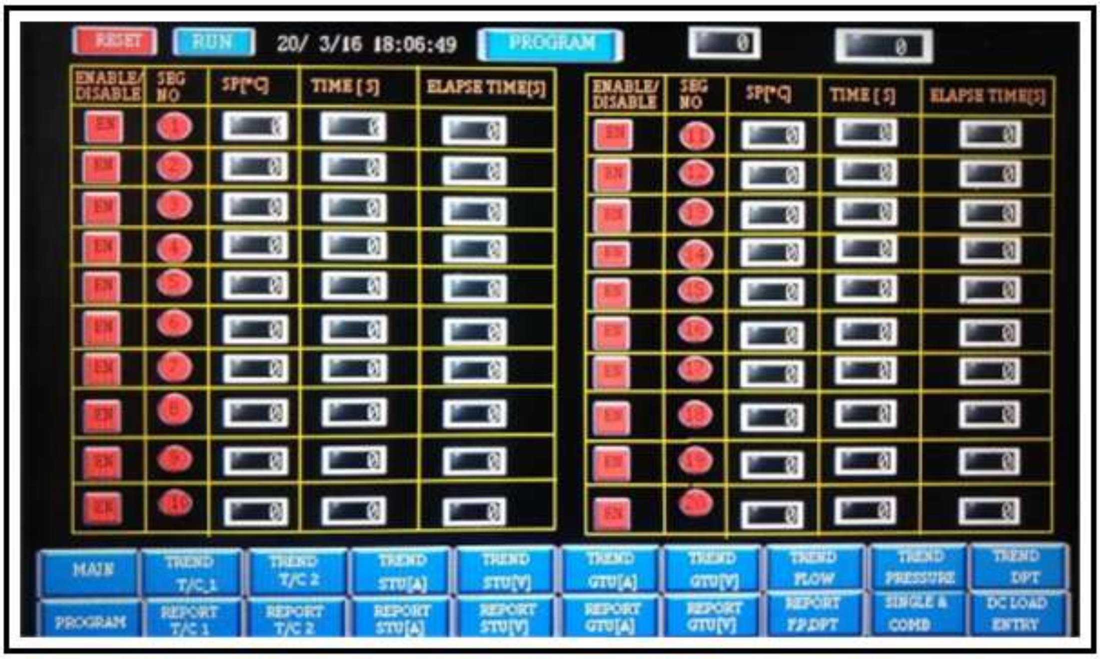

Fig. 4.2 Input command entry page of the program

The THST was changed from 50°C to 300°C at a rate of 50°C per minute in the initial TCP (TCP1). Similar to TCP1, the THST of the second TCP (TCP2) ranged from 50 to 300 degrees Celsius, but the heating rate was raised to about 85 degrees Celsius per minute [11]. For the third TCP (TCP3), the air heating rate was kept at 50°C per minute while the THST was adjusted between 50°C and 350°C. The three TCPs are depicted in Figure 4.2, and each TCP's THST and air heating rate are listed in Table 4.1. The TE modules underwent 150 thermal cycles in TCP1 and TCP2, and 300 cycles in TCP3. Ten minutes was the dwell period in each of the three scenarios.

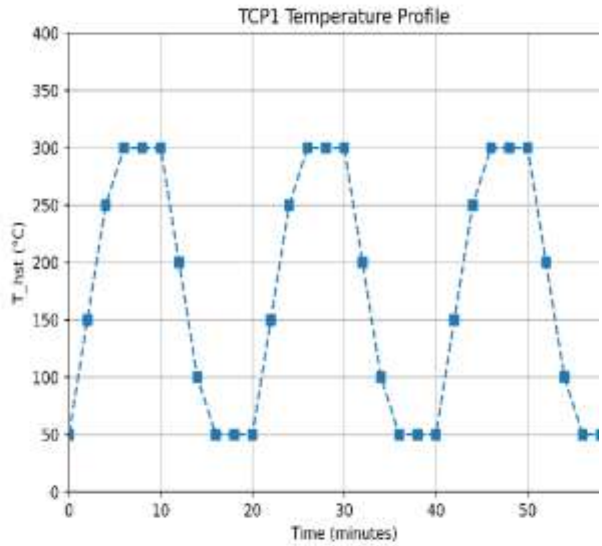

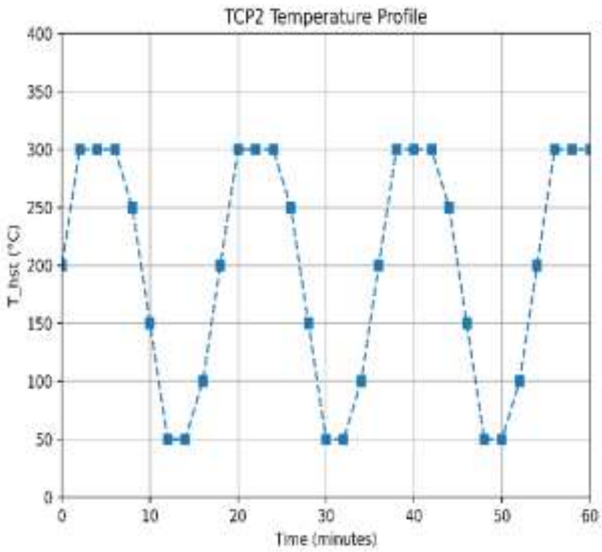

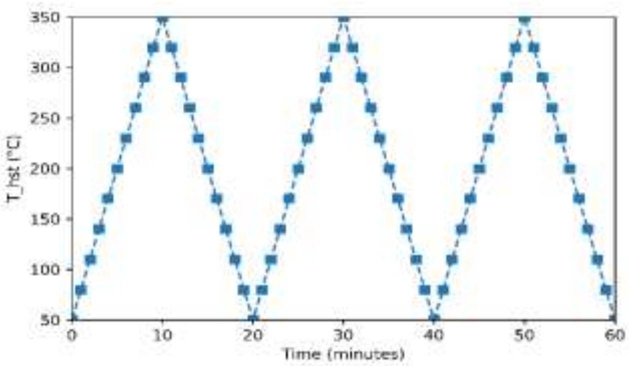

Fig. 4.3 (a) Thermal cycling profile 1 (TCP1), (b) Thermal cycling profile 2 (TCP2) and (c) Thermal cycling profile 3 (TCP3)

Table 4.1 Thermal cycling profile parameters

Thermal cycling profile	**Heater set temperature, THST (°C)**	**Heating rate (°C/min)**	**Dwell time at THST (minutes)**
TCP1	300	50	10
TCP2	300	85	10
TCP3	350	50	10

5. RESULTS AND DISCUSSIONS

5.1. Temperature variation and heating rate of the TE modules

The ~Th values measured under steady state settings that correlate to each TCP's maximum THST (holding temperature) are displayed in Figure 4.3(a). For all three TCPs, it was found that ~Th values exhibited the same tendency. Along the direction of hot airflow, the ~Th values displayed a declining trend. This behavior was comparable to what was seen when mapping surface temperatures [12]. Figure 4.3(b) shows the heating rate of the individual TE modules at eight different locations on the heat exchanger surface, determined from the slope of the heating obtained from corresponding ~Th values [13]. Along the hot airflow's streamwise direction, the heating rate likewise dropped. The average heating rate of TE modules under TCP1 and TCP3 was found to be about twice that of TE modules under TCP2. The shorter residence period of hot air within the heat exchanger may be the cause of the TE modules decreased heating rate under TCP2, despite the air's quick heating rate (85°C/min) to the preset temperature in comparison to TCP1 and TCP3. Additionally, it was noted that the current study's module heating rate was significantly lower than that of the conduction setup-based tests reported in the literature [1], [2], and [3]. This would result in a slower degradation rate of the TE modules as it is proportional to the module heating rate [1].

Table 5.1. Variation of heating rate across thermoelectric module positions for different temperature cycling profiles (TCP1–TCP3).

Position	**TCP1**	**TCP2**	**TCP3**
1	**278**	**266**	**314**
2	**258**	**260**	**296**
3	**232**	**248**	**242**
4	**256**	**231**	**272**
5	**251**	**245**	**266**
6	**250**	**238**	**255**
7	**253**	**218**	**266**
8	**168**	**215**	**182**

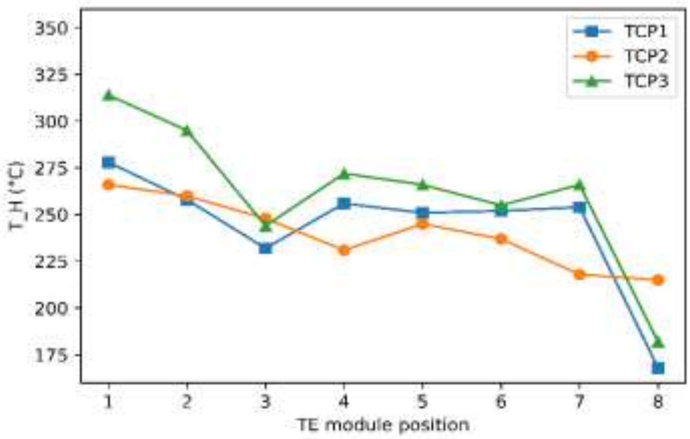

Table 5.2. Experimental heating rates at various TE module locations under three temperature cycling protocols.

Position	**TCP1**	**TCP2**	**TCP3**
1	9.5	5.8	10.5
2	11	5.5	9.1
3	9.8	5.5	10.2
4	9	4.9	8.6
5	7.8	4.2	7.6
6	8.3	4.1	8.3
7	7.1	3.6	7.6
8	4.8	3.9	5.4

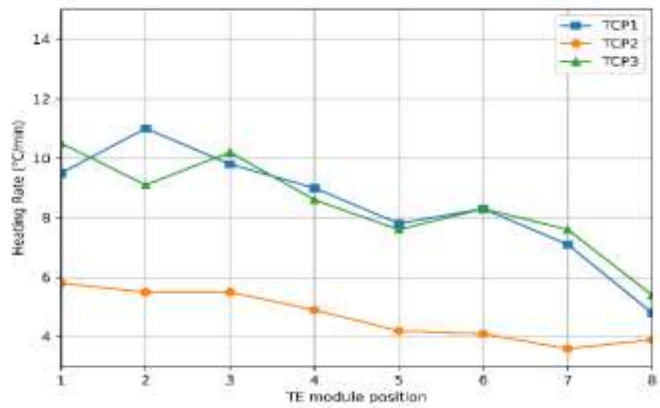

Fig. 5.3 (a) ~Th values measured adjacent to each TE module position at the steady state conditions corresponding to the maximum THST of each TCP before thermal cycling (b) Heating rate of the modules at different positions on the heat exchanger surface when the inlet air is heated at 50°C/min (TCP1 & TCP3) and 85°C/min. (TCP2) [2]

6. CONCLUSION

In this work, an automotive exhaust thermoelectric generator (AETEG) for light-duty vehicle applications was designed, manufactured, and tested. AETEG performance was assessed experimentally under steady state and thermal cycling circumstances in a specially designed, sturdy, and compact hot air-based test apparatus. The thermal behavior of the heat exchanger and the electrical performance of the arrays of TE modules was assessed under different operating conditions. The following are the main findings from the experimental investigations conducted in this work:

1. According to the temperature distribution mapping on the heat exchanger surface, the average surface temperature peaked 75 mm from the rectangular channel's intake and then dropped as it approached the outlet. Thermal insulation reduced the spatial fluctuation in temperature.
2. The maximum efficiency obtained for the present pin-fin heat exchanger design was 9.2% in bare condition at hot air inlet temperature (TiH) of 385°C and a hot air mass flow rate (MFR) of 260 kg/h. However, after assembling it in AETEG with 44 TE modules, it was 12.7%. The increase in the latter case was due to forced heat extraction from the heat exchanger by the cooler plates through the TE modules which resulted in a lower hot air outlet temperature (T_oH) value.
3. At the maximum T_iH of 385oC and hot air MFR of 255 kg/h, the heat exchanger caused a maximum pressure drop of 0.9 kPa. This pressure drop was within an AETEG's permissible range. The expansion and contraction losses from the truncated pyramidal structures and the perforated plate placed at the heat exchanger's rectangular channel input were the main causes of the pressure reduction.
4. Due to temperature mismatch conditions, the TE modules delivered varied VOC and Pmax for a given heat input depending on where they were on the AETEG. Eight TE modules produced more power than twenty-four TE modules under same heat input and experimental conditions. The percentage occupancy of the TE modules over the heat is indicated by this observation.

7. REFERENCES

[1] A. Gabriel-Buenaventura, J. H. Martínez, and A. García, “Energy recovery techniques in automobiles: A review,” *Renewable and Sustainable Energy Reviews*, vol. 49, pp. 813–824, 2015.

[2] N. Sahiti, A. Lemouedda, and F. Durst, “Thermal performance comparison of pin fin heat exchangers with different pin cross-sections,” *Appl. Therm. Eng.*, vol. 26, pp. 1176–1185, 2006.

[3] O. von Wilmersdorf and J. S. Weigand, “Heat transfer and pressure drop in pin-fin heat exchangers for gas turbine cooling,” *Int. J. Heat Mass Transf.*, vol. 50, pp. 1889–1899, **2007.**

[4] Z. Chen, Q. Li, D. Meier, and H. J. Warnecke, “Convective heat transfer and pressure loss in rectangular ducts with drop-shaped pin fins,” *Heat and Mass Transfer*, vol. 33, pp. 219–224, 1997.

[5] H. Li, T. Kumada, and M. Faghri, “Experimental investigation of heat transfer in channels with elliptical pin fins,” *Int. J. Heat Mass Transf.*, vol. 41, pp. 421–431, 1998.

[6] A. Pandit, S. Joshi, and P. K. Sharma, “Experimental study of heat transfer characteristics of pin-fin arrays under varying Reynolds numbers,” *International Journal of Thermal Sciences*, vol. 82, pp. 48–57, 2014.

[7] S. C. Tzeng, C. H. Chen, and Y. L. Huang, “Performance analysis of thermoelectric generators integrated with metal pin-fin heat exchangers,” *Energy Convers. Manag.*, vol. 84, pp. 553–560, 2014.

[8] M. K. Chyu, C. H. Yen, and S. Siw, “Comparison of heat transfer from staggered pin-fin arrays with circular, cubic and diamond-shaped elements,” in *ASME Turbo Expo 2007: Power for Land, Sea and Air*, Montreal, Canada, 2007, pp. 1–9.

[9] K. Bilen, U. Akyol, and S. Yapici, “Heat transfer and friction correlations for finned surfaces and thermal performance analysis,” *Energy Convers. Manag.*, vol. 42, pp. 1071–1083, 2001.

[10] S. Hatzikraniotis, T. Kyratsi, and K. M. Paraskevopoulos, “Thermal cycling effects on the reliability of thermoelectric modules,” *J. Electron. Mater.*, vol. 38, pp. 1173–1181, 2009.

[11] S. Park, H. Lee, and J. Kim, “Flexible thermoelectric generator for human body heat energy harvesting,” *Adv. Funct. Mater.*, vol. 30, no. 19, p. 1906257, 2020, doi: 10.1002/adfm.201906257.

[12] C. Merienne, P. D. Phelan, and S. Graham, “Thermal cycling degradation mechanisms in thermoelectric modules,” *J. Electron. Mater.*, vol. 48, pp. 356–364, 2019.

[13] S. Harish, R. R. Kumar, and P. R. Kumar, “Experimental investigation of temperature distribution and heating rate in thermoelectric modules for waste heat recovery applications,” *Energy Convers. Manag.*, vol. 245, p. 114548, 2021.